Modeling the breakup stage of relativistic heavy-ion collisions

Scott Pratt and Joelle Murray

Department of Physics and Astronomy and

National Superconducting Cyclotron Laboratory,

Michigan State University, East Lansing, MI 48824 USA

(October 10, 1997)

Abstract

By using the output of a thermal model as the input to a hadronic cascade, we investigate the role of kinetic and chemical equilibrium in the breakup stage of $158 \cdot A$ GeV/c Pb + Pb collisions at CERN. Gross features of experimental pion and proton spectra are fit, as well as the transverse energy and baryons per unit rapidity. However, experimental source sizes extracted from pion correlations and the low p_t behavior of pion spectra are not reproduced. We argue that pionic phase space has become over populated compared to equilibrium considerations. Other issues regarding chemical and kinetic equilibration are also explored.

I. INTRODUCTION

Heavy ion collisions at relativistic energies create an environment where energy and particle densities are sufficiently high to alter the normal state of matter. One fm/c after a collision of 158A GeV/c Pb ions at CERN, energy densities probably exceed 2.0 GeV/fm^3 [1–3]. At such densities, normal hadronic degrees of freedom should be irrelevant as the number of hadrons per cubic Fermi exceed the inverse size of a typical hadron. As the collision's expansion lowers the density, and hadrons become appropriate degrees of freedom, chiral symmetry might still be partially restored thus greatly altering masses and other hadronic properties [4]. Unfortunately, we are shielded from these most interesting stages of the collision by the final breakup stage of the collision. Hadrons collide several times before the system reaches breakup energy densities near 50 MeV/fm^3. The breakup process, which is closest to measurement, must be well understood before confident inferences can be made regarding earlier stages. Electromagnetic probes, such as electrons and photons, can escape before the breakup stage and perhaps unveil information regarding the more mysterious forms of matter. However, even in the analysis and interpretation of such probes, constraints imposed by hadronic measurements regarding entropy density, size, and collective expansion strongly affect the conclusions.

For this reason we embark on an investigation of the breakup process in heavy-ion collisions. Our initial goal is modest. We wish to understand the validity of thermal concepts through simulating the evolution and decoupling of a locally equilibrated, but expanding, hadronic gas. In the next section we describe the prescription for a thermal model that includes surface emission. This model is in the same spirit as other models [5–8]. The following section then describes a cascade code used to simulate interactions of the thermally generated particles. The combination of thermally generated particles with the cascade prescription will be referred to as the BNC (burn and crash) model. Section IV describes the way in which experimental measurements are used to determine the parameters in the models. The six subsequent sections discuss physics issues: collective flow, chemical equilibration of pions, the role of surface emission, sensitivity to cross sections, the validity of kinetic equilibrium and nucleonic source size measurements respectively. Despite the flexibility of the models presented here, we fail to satisfactorily reproduce experimental results, even when thermal considerations are applied to early stages of the collision and a cascade description is used to model the subsequent evolution. Notably, experimentally determined source sizes appear smaller than those predicted here, and emission appears to occur more suddenly and less surface-like. The lessons learned from these exercises are presented in section XI.

II. FREEZEOUT OF AN EXPANDING ELLIPSE

Most freezeout models describe freezeout in terms of the same variables: temperature T, chemical potentials μ_i, sidewards size R, and transverse velocity $v_\perp$. But models vary widely in the details, such as the shape of the breakup hypersurface and the velocity profile. For our model we choose to use a purely space-like hyper-surface, meaning that in the local frame of the expanding matter, the breakup appears locally instantaneous. This means that if an observer is traveling in a small cell that moves along with the expanding matter, the breakup will occur on both sides of the cell simultaneously. The breakup hypersurface is specified by giving the breakup time as a function of position, $t_b(\mathbf{r})$. For the breakup to be locally instantaneous in the frame of the matter that moves with velocity $\mathbf{v}$,

$$\nabla \mathbf{t}_b(\mathbf{r}) = \mathbf{v}, \tag{1}$$

where it is assumed that $c = 1$. A second ansatz is that the matter not accelerate. This means that if one follows an element of matter through time, the element's velocity remains constant,

$$\left(\frac{\partial}{\partial t} + \mathbf{v}\cdot\nabla\right)\mathbf{v} = \mathbf{0} \tag{2}$$

Mayer and Heinz [5] have recently introduced a model where a non-zero acceleration has been considered that is intermediate between a simple thermal parameterization and a full hydrodynamic prescription.

One example of a surface that satisfies these criteria is the Bjorken description of a one-dimensionally expanding tube.

$$t = \sqrt{\tau^2 + z^2}\ , \quad \mathbf{v} = \frac{z}{t}\hat{z} \tag{3}$$

Another example is the three-dimensional expansion used to describe cosmological expansion in the limit gravity is neglected.

$$t = \sqrt{\tau^2 + x^2 + y^2 + z^2}\,, \quad \mathbf{v} = \frac{\mathbf{r}}{t}\ . \tag{4}$$

Both these examples are boost-invariant as long as all local observables, e.g. density and temperature, depend only on τ, referred to as the proper time, the time measured by a local comoving observer. The Bjorken model is invariant to boosts along the z-axis (beam axis) while the three-dimensional model is invariant to boosts in any direction. Boost-invariance implies that all comoving observers will view identical evolutions of local observables. Boost invariance also implies zero acceleration.

The collective velocity profile presented here incorporates both transverse and longitudinal (along the beam axis) expansion but allows the velocity gradients to be different between the transverse and longitudinal direction. It also satisfies Eq.s (1) and (2) above. The time t at which one reaches a certain proper time τ is:

$$t^2 = \left(\sqrt{(\tau + t_0)^2 + x^2 + y^2} - t_0\right)^2 + z^2. \tag{5}$$

The resulting collective velocities, $\mathbf{v}$, and four-velocities, $\mathbf{u} = \gamma\mathbf{v}$, using Eq. (1) are:

$$\begin{aligned} v_z &= \frac{z}{t}\ ,\ u_z = \frac{z}{\sqrt{\tau_z^2 - (x^2+y^2)\cdot\frac{\tau_z^2}{(\tau_z+t_0)^2}}}\ , \\ v_x &= \frac{\tau_z}{\tau_z + t_0}\cdot\frac{x}{t}\ ,\ u_x = \frac{x}{\tau + t_0}\ , \\ v_y &= \frac{\tau_z}{\tau_z + t_0}\cdot\frac{y}{t}\ ,\ u_y = \frac{y}{\tau + t_0}\ , \end{aligned} \tag{6}$$

where τ_z is usual Bjorken proper time, $\tau_z^2 \equiv t^2 - z^2$. For large proper times this case approaches the isotropic case in Eq. (4) and for short times corresponds to the Bjorken longitudinal-expansion case shown in Eq. (3). The parameter t_0 regulates the difference between the sidewards and longitudinal velocity gradients. Whereas the longitudinal gradient is always the inverse time, the transverse gradient must start lower due to the large initial transverse size. The time t_0 can be thought of as a head start for the sidewards size as compared to the longitudinal size.

It should be emphasized that this parameterization is rather arbitrary. For instance, one might have chosen the transverse velocity to increase linearly from the axis instead of the four-velocity. This would become important for relativistic transverse velocities but for our case the velocities tend to be near half the speed of light. More importantly, the choice of breaking up the matter at a given proper time affects the correlation function. This parameterization has an inside-outside characterization both transversely and along the beam directions, with the inside dissolving slightly before the outer matter. However, for a given value of z disintegration is nearly simultaneous since sidewards velocities are not fast compared to c. To make the model more physical, evaporation from the surface has been added. Of course, a more realistic model would incorporate a non-uniform density profile [9]. For the simple model here, we assume all matter inside the elliptical surface is at a fixed density and temperature in the rest frame of the matter.

Another choice must be made with respect to the shape of the surface. We choose a non-accelerating surface defined by

$$\frac{u_x^2 + u_y^2}{u_{\perp,\max}^2} + \frac{u_z^2}{u_{z,\max}^2} = 1 \ , \tag{7}$$

where the positions are defined according to the Eq. (6). By using Eq.s (6), one can translate this surface to coordinate space. In coordinate space the ellipse starts out as a pancake for times much shorter than t_0, but becomes prolate along the z-axis at later times.

Finally, the local breakup is defined thermally according to the temperature T, the baryon chemical potential μ_b, the strangeness chemical potential μ_s, and the chemical potential for conserving electric charge, μ_Q. The latter two chemical potentials were chosen to be zero. This gives a slight net strangeness due to the presence of baryons. As we are not concerned with strangeness equilibrium in the present work, it has little affect. Since the initial gold nuclei have more neutrons than protons, the electric chemical potential should also be non-zero. We ignore this fact for this work and model isospin-symmetric matter.

The time t_0 was chosen to give a transverse size $R_0 = 6$ fm for $t = 0$ when $z = 0$. Manipulating Eq. (6) with $t = 0$, $z = 0$ and $v_\perp = v_{\perp,\rm max}$, it can be shown that this condition becomes

$$v_{\perp,\rm max} = \frac{R_0}{t_0}\ . \tag{8}$$

Rather than referring to t_0, we will refer to $v_{\perp,\rm max}$. The final transverse size is then determined by the proper breakup time τ_b.

In summary, there are five free parameters given that the initial transverse size is fixed at 6.0 fm and the strangeness chemical potential is set to zero. The strangeness chemical potential should have a small value given the presence of a net baryon number, but we will ignore it given that strangeness equilibration will not be considered in this study. The five adjustable parameters are: T, $v_{\perp,\rm max}$, $v_{z,\rm max}$, μ_b and τ_b.

Evaporation from the surface was included by assuming a black-body form. The temperature of the surface was assumed to be identical to the final bulk breakup temperature. The chemical potential μ_b of the matter at the surface is also assumed to be the same as the final chemical potential. Emission from the surface is modeled by thermally generating particles within a distance $c\Delta t$ of the surface, then allowing them to escape according to the weight, $\mathbf{v}\cdot\hat{r}\Theta(\mathbf{v}\cdot\hat{r})$, where $\hat{r}$ is a unit vector directed away from the surface and v is the velocity of the particle. Since conditions at the surface might be quite different than final breakup condition, firm quantitative conclusions are not warranted. However, one can gain important qualitative lessons and a rough quantitative understanding of the evaporative contribution.

Only the lowest lying hadrons, those that do not represent orbital excitations of quarks, were included in the statistical generation of the events. Given that the model is meant to be taken seriously only when temperatures are below 160 MeV, the neglect of higher mass resonances is warranted. A list of the particles and their masses is given in Tables I and II.

Particles and resonances were generated via Monte Carlo, and resonances were subsequently decayed. The space-time points of the created particles were stored for later consideration by the cascade simulation or for the purposes of generating correlation functions.

III. THE HADRONIC CASCADE SIMULATION

There already exist several well developed hadronic cascades which are appropriate for modeling heavy-ion collisions at CERN energies. Three such models are RQMD [10], VENUS [11] and QGSM [12]. These models are all much more sophisticated treatments than what we present here, as they include a description of the entire collision, including the creation of hadrons from initial nucleon-nucleon collisions. Since our primary goal is to understand the implications of scattering and thermalization and to determine quantities such as the temperature and density due to fitting, we are most interested in a fast and flexible simulation that would allow one to more fully explore the parameter space.

This cascade considers only elastic scatterings, fusions and decays. Most notably, inelastic two-to-two processes are neglected except for when two particles fuse to form a resonance then decay into different particles. The neglected processes might be important for considering issues regarding chemical equilibrium, e.g. $p\pi \leftrightarrow \Lambda K$ would be necessary for understanding strangeness equilibrium. We also exclude highly inelastic collisions where subsequent string decay may create multiple hadrons. However, the lack of more sophisticated processes should not be crucial given that the goals of the current study are confined to issues of kinetic equilibrium at the last stage of the reaction where two-body scatterings rarely have relative kinetic energies greater than a GeV.

Elastic scatterings are given energy-independent cross sections of 8, 12 and 16 mb for hadron-hadron, hadron-baryon and baryon-baryon collisions respectively. The reaction plane is preserved in the scattering, and the polar angle of the scattering is chosen randomly (rather than choosing $\cos\theta$ uniformly). In a classical picture such an angular distribution amounts to filling phase space under the constraints of angular momentum and energy conservation. The two particles change their trajectories in the scatterings at space-time points x_1 and x_2 such that in their center-of-mass frame, the alterations of the trajectories occur simultaneously as they come abreast of one another.

The cross section for fusions $A+B\rightarrow C$ are chosen with a simple Breit-Wigner shape.

$$\sigma = \frac{\pi\cdot f_{ab}}{q_R^2}\frac{(2J_c+1)}{(2J_a+1)(2J_b+1)}\frac{(\hbar c\Gamma)^2}{\left(\frac{\Gamma}{2}\right)^2+(m-m_c)^2} \tag{9}$$

The widths were chosen to be energy independent and the branching ratios, f_{ab}, were taken from experiment. The relative momentum of the fusing particles at resonance is q_R. The decays of the particles was chosen with an energy independent lifetime, Γ^{-1}, and the decay into various branches was chosen according to the branching ratios f_{ab}. A resonance formed by such a fusion does remember the relative position of the two-particles which created it. When the resonance decays, the two created particles are separated by this same amount. This prevents fusions and decays from collapsing the system. This prescription for treating the decays and fusions will effectively populate resonances according to the density of states of the resonance if the width of the resonance is small compared to the kinetic energy of the decaying products. The facts that the decaying resonance retains no identity of the particular channel that fed it, and that the cross sections do not have the correct form near threshold are shortcomings. A more consistent treatment of such scattering is certainly possible, but would require a more sophisticated approach [13].

The algorithm used for the cascade is event based. Newly created particles are tested for all possible future decays and scatterings. If a future scattering or decay is possible, it is added to an event list which is ordered by time. The ordering of the events unfortunately requires the choice of a reference frame. This is chosen to be the center-of-mass frame of the entire system. For scatterings, which alter trajectories of the two particles at slightly different times due to relativistic effects, the average of the two times is assigned to the event for purposes of time-ordering. Although individual scatterings are unaffected by the reference frame of the description, the ordering of the events is frame dependent. However, as long as the mean free path is large compared to typical impact parameters for scattering (≈ 1.0 fm), there should be little frame dependence. Since only the breakup stage of the collision is considered here, event ordering should not be an issue as it would be for simulations which describe the early stage of a relativistic heavy ion collision. The simplicity of this approach allows for rapid generation (approximately 15 seconds per event with a 200 MHz work station) of events, which makes exploration of the 5-dimensional parameter space tenable.

IV. FITTING PROCEDURES

The thermal model has five free parameters, given that the transverse size of the tube was fixed at 6 fm for $\tau = 0$. The parameters are the maximum collective transverse velocity $v_{\perp,\max}$, the maximum collective velocity along the beam axis $v_{z,\max}$, the temperature T, the baryon chemical potential μ_b and the breakup time τ. The excess of neutrons to protons is neglected as is the small strangeness chemical potential necessary to keep the net strangeness at zero in an environment where there are more baryons than antibaryons. For a more ambitious study, where strangeness equilibrium is of interest or where Coulomb distortions to spectra were considered, the additions of two extra chemical potentials could be included.

The five parameters were chosen to reproduce preliminary Pb+Pb experimental results. First a temperature T was arbitrarily chosen. Next μ_b, τ, and the two velocities were chosen to reproduce four fixed results: a transverse energy per unit rapidity, $dE_t/dy = 390$ GeV [1], a number of nucleons per unit rapidity $dN/dy = 75$ [3], a charged particle rapidity distribution $dN_c/d\eta$ which had a variance of 1.35 [3], and an effective pion temperature of 165 MeV [14,3]. Since the neutron-to-proton excess of Pb is neglected in our present considerations, we chose to produce a slightly higher number of protons per unit rapidity than were measured. We must emphasize that the actual shape of preliminary pion spectra from NA44 and NA49 were not reproduced. The NA44 collaboration has measured the spectra for p_t (0-700 MeV/c) [14], while the NA49 collaboration has made measurements at the higher end of this range. The measurements reveal a distinctly non-exponential shape to $dN/(p_t dp_t dy)$ with a much sharper peak at the origin than what we can explain with our thermal model. The effective temperature extracted from our model results is taken by choosing T_{eff} such that an exponential slope, $dN/(p_t dp_t dy) \propto e^{-E_\perp/T_{eff}}$, would result in an average transverse energies per pion in a fixed rapidity window equal to what is extracted from our model.

Fitting the four parameters (The temperature T being chosen already) to four experimentally motivated values is not difficult since there is a tight correspondence of each model parameter with a single experimental value. The baryon chemical potential, μ_b, is tied to $dN_{nucleon}/dy$; the transverse velocity, $v_{\perp,\max}$, determines T_{eff}; the breakup time, τ, determines dE_t/dy; and the maximum longitudinal velocity $v_{z,\max}$ is related to the variance of $dN_c/d\eta$. This nearly one-to-one correspondence along with the monotonic dependencies ensures that the fit of parameters is unique. We only consider measurements at mid-rapidity. Any reasonable global analysis would surely incorporate chemical potentials and temperatures that were rapidity dependent. Tolerances for the fit quantities were: ± 1.0 MeV for T_{eff}, ± 1 for $dN_{nucleon}/dy$, ± 5.0 GeV for dE_t/dy, and ± 0.05 for σ_y when 100 events were used to generate the results.

For the studies in this paper, four different classes of models were considered.

I. Thermal model with no evaporation or cascade. Breakup temperatures were 100, 120 and 140 MeV.

II. Thermal model, with evaporation included, but no cascade. Breakup temperatures were 100 120 and 140 MeV.

III. BNC model, a thermal model with both evaporation and cascade included. Breakup temperatures were chosen to be 120, 140 and 160 MeV.

IV. Same as III, only with the elastic cross-section reduced by a factor of two. Only the T=160 MeV case was considered.

Parameters are shown in table III. In the following sections, the validity of the issue of thermalization will be addressed. The parameters are meaningless if they refer to a stage of the collision where local equilibrium is lost. Nonetheless, determination of the parameters is necessary to check the self consistency of the thermal hypothesis.

V. DETERMINING COLLECTIVE FLOW

A principal goal in studying ultrarelativistic collisions is to understand the equation of state of hot and dense matter. The pressure manifests itself through the conversion of thermal energy into collective energy as the system expands. Thus determining the collective velocity is crucial for understanding the equation of state.

The final collective velocity can not be determined by viewing spectra of a single species. Even collisionless gases expand and go through an apparent cooling as the spread in the local velocity falls with time. However, by viewing the spectra of two species with different masses, one can then infer the final collective velocity. For our study, we will focus on pions and nucleons. Nucleons, due to their greater mass, have small thermal velocities and their spectra is more greatly affected by collective flow. We neglect kaons for the current study, although the information inferred from comparing pions with nucleons could be inferred from comparison of pion with kaons although with less sensitivity.

As mentioned in the previous section the fitting procedure involves choosing $v_\perp$, μ_b, τ_b and $v_{z,\max}$ from four experimental constraints which leaves the temperature as a free variable. Pion and proton spectra are shown in Fig.s 1 and 2 respectively. The left panels show spectra for the thermal model without evaporation or subsequent treatment with the cascade. The center panels include evaporation and the right panels include scattering of the thermally generated particles via a cascade prescription. All spectra were generated with 100 events and by binning particles within one unit of mid-rapidity. Since Coulomb and isospin effects have been excluded, all three isospin species were used.

The models reproduce experimental pion spectra at momenta above 200 MeV/c, but under predict the experimental result by approximately a factor of two at $p_t = 0$. The models produce remarkably similar pion spectra. Although Bose effects were included for the thermal and evaporative calculations, they were not considered for the input into the cascade code. The failure of the models at low p_t and the influence of Bose effects will be discussed again in section VI.

Proton spectra are shown in Fig. 2. All model parameters were already set in fitting the pion spectra. For simple thermal model without evaporation, a reasonable fit for the spectra only occurs when a breakup temperature of 120 MeV is assumed. Higher breakup temperatures require lower collective transverse velocities to fit the pion spectra, and then fail to provide sufficient boost to protons. The maximum transverse collective velocity in this case is 65% the speed light.

Evaporation affects nucleons only weakly, since slow heavy particles are unlikely to evaporate from the surface. Evaporation strongly affects the pion spectra. By including evaporation, one can choose a lower transverse velocity for a given breakup temperature to fit the pion spectra. This is the expected result, since evaporated particles move faster than the surface. The result is that in order to obtain a sufficiently hot proton spectra, one must lower the breakup temperature. As shown in Fig. 2, a breakup temperature of 100 MeV is consistent with data when evaporation is included in the model. However, as will be demonstrated in Section VII such a low temperature corresponds to an extremely dilute gas which is inconsistent with expectations of breakup densities based on hadronic scattering rates.

Including the cascade treatment is remarkably successful at consistently reproducing the proton spectra for a range of temperatures from 120 to 160 MeV. This suggests that the cascade consistently reproduces the sidewards flow by beginning the simulation at earlier times. Surprisingly, this even worked at a temperature of 160 MeV, where the assumptions inherent in the cascade are questionable. For the moment, the fit to the proton spectra with the cascade treatment suggests a system that stays in equilibrium in the range of 120 to 160 MeV. Table III then suggests that the sidewards collective velocity accelerates from $0.320c$

to $0.485c$ as the local temperature falls from 160 to 120 MeV. Given that this velocity is still smaller than the thermal velocity of a pion at 120 MeV, this suggests the bulk of energy remains as thermal energy.

It should be emphasized that the conditions for the breakup at this point have been based on the assumption of pionic chemical equilibrium. The validity of such an assumption is the subject of the next section.

VI. CHEMICAL EQUILIBRATION OF PIONS

Chemical equilibrium might not be attained during the hadronic stage of a heavy-ion collision. For pions, chemical equilibrium can be thought of as the equilibration of the number density of hadrons given the local kinetic temperature. Using the BNC model (thermal + cascade), as described previously, allows one to infer the geometry and collective velocity of earlier stages of the collision. However, these inferences relied on the unquestioned assumption that chemical equilibrium was maintained to the time particles are thermally generated.

Correlation measurements allow one to test the assumption of pionic chemical equilibrium by providing insight into the volume. The final volume has been set largely by the condition that the net transverse energy is 390 GeV per unit rapidity. Should the model's correlation functions fit experimental correlation functions, one would have verification of the chemical equilibrium hypothesis.

First we present calculations of pionic source sizes through correlation measurements. Correlations were calculated for pion pairs at mid rapidity and binned according to the average p_t of the pair. The p_t bins are of 100 MeV/c width and are noted by $\bar{p}_t$:

$$-0.5 < y_{pair} < 0.5, \quad y_{pair} \equiv \frac{1}{2} \log \frac{E_1 + e2 + p_{z,1} + p_{z,2}}{E_1 + e2 - p_{z,1} - p_{z,2}} \tag{10}$$

$$\bar{p}_t - 50\text{MeV/c} < \frac{p_{\perp,1} + p_{\perp,2}}{2} < \bar{p}_t + 50\text{MeV/c} \tag{11}$$

Correlations were calculated by weighing pairs with a symmetrization weight $1 + \lambda \cos(p_2 - p_1) \cdot (x_2 - x_1)$. Three dimensional correlations were then calculated in the rest frame of the pair in relative momentum bins of size 2 MeV/c by 2 MeV/c by 2 MeV/c. They were then fit to a simple three-dimensional Gaussian in the region $|\mathbf{q}| < 100$ MeV/c.

$$C(\mathbf{p},\mathbf{q}) = 1 + \exp\left\{-q_{out}^2 R_{out}^2(\mathbf{p}) - q_{side}^2 R_{side}^2(\mathbf{p}) - q_{beam}^2 R_{beam}^2(\mathbf{p})\right\} \tag{12}$$

$$q_{out} \equiv \frac{\mathbf{q}_\perp \cdot \mathbf{p}_\perp}{|\mathbf{p}_\perp|}$$

$$q_{side}^2 \equiv \mathbf{q}_\perp^2 - q_{out}^2$$

$$q_{beam}^2 \equiv q_z^2 - q_0^2 + \frac{(p_0 q_0 - p_z q_z)^2}{p_0^2 - p_z^2}$$

The total and relative momenta are $\mathbf{p}$ and $\mathbf{q}$ respectively. The beam axis is assumed to be along the z direction.

Correlation functions were generated by simulating 2×10^7 pairs with relative momenta less than 100 MeV/c. Fig. 3 shows an example of a calculated correlation function compared to the fit function. The model correlation functions were projected in the outwards, sidewards and beam directions by requiring the relative momentum to be within 30° of the chosen direction. One can see that the correlation functions are not extremely Gaussian, and that the fit λ parameter thus underestimates the true intercept. Since weak decays decays were not considered as source points for pions, the fact that the correlation function does not go to 2.0 at $\mathbf{q}$=0 is primarily due to η decays.

Fig. 4 shows the gaussian radii as a function of the average transverse momentum for both the T=120 case and the $T = 160$ case. The sizes are noticeably smaller in the sidewards direction. For the T=160 MeV case the outwards size is noticeably larger than experimentally extracted numbers. This suggests that emission occurs more suddenly than what is expected from the model. Further interpretation of this comparison to experimental results is presented in the conclusions. The fact that the T=120 MeV case is more inconsistent with experiment is explained below.

Isentropic expansions at fixed pion number do lead to over population of the pion's phase space [15,16]. Resonance decays can also contribute. Processes that significantly change the overall pion number (A ρ meson can be counted as two pions so that its creation and decay does not change the overall pion number.) are neglected in the cascade. The most important channel for reducing the pion number should be $\rho\rho \to \pi\pi$, but this should not change the overall pion number by more than a few percent for temperatures below 160 MeV.

If the phase space for pions is significantly over populated, Bose effects can significantly enhance spectra at low p_t. Indeed, pion spectra at low p_t were under predicted in the previous section by approximately a factor of two. Bose effects had not been included in the model considerations for the cascade cases considered thus far. One expects Bose effects to enhance the spectra by modifying the phase space occupation:

$$f(\mathbf{p},\mathbf{r},t) \to \frac{f_0(\mathbf{p},\mathbf{r},t)}{1-f_0(\mathbf{p},\mathbf{r},t)}, \tag{13}$$

where f_0 is the phase-space-filling factor where Bose effects were neglected. Bertsch [17] showed how correlation functions can be used to extract the average phase space density through a sum rule.

$$\begin{aligned}\bar{f}(\mathbf{p}) &\equiv \frac{\int d^3r f(\mathbf{p},\mathbf{r},t)^2}{\int d^3r f(\mathbf{p},\mathbf{r},t)} \\ &= \frac{dN}{2\pi m_\pi \; p_t dp_t dy}\int d^3q_{inv}\left(C(q_{inv})-1\right)\end{aligned} \tag{14}$$

The average is over coordinate space, and the time t is assumed to be a breakup time.

We apply these considerations to estimate the Bose effects on the spectra. By calculating correlation functions at mid-rapidity as a function of p_t, one can use Eq. (14) to estimate $\bar{f}_0$ as a function of p_t which is presented in Fig. 5. Two cases are illustrated, the case where a cascade is applied to thermally generated particles at T=120 MeV and the same with particles generated at 160 MeV. The average phase space occupation for the 160 MeV case is approximately 20% higher than the 120 MeV case where particles were created approximately at breakup density. This demonstrates that in the BNC model beginning at 160 MeV, pion phase space becomes over populated by approximately 20% during the expansion. This is in accordance with what one expects in an isentropic expansion where the overall pion number is fixed aside from decays of resonances. The 20% excess can be quantified as an effective chemical potential of approximately 25 MeV.

One can estimate Bose corrected spectra via the relation:

$$\frac{dN}{2\pi m_\pi\ p_t dp_t dy} = \frac{dN_0}{2\pi m_\pi\ p_t dp_t dy} \cdot \frac{1}{1 - \bar{f}_0(\mathbf{p})}, \tag{15}$$

The corrected spectra are shown in the lower panel of Fig. 5 for the T=160 MeV case described above. The spectra are magnified by approximately 30% at low p_t although a factor of two would be necessary to agree with the experimental results. Experimental correlation functions shown in Fig. 4 also show a more compact source than those resulting from the BNC model. Since all three dimensions of the source sizes affect the phase space density, the apparent volume (the product of the three dimensions) appears larger by approximately a factor of two as compared to the NA49 results. One way of stating the result is that the thermal model can account for an effective chemical potential of 25 MeV, but that experimental results suggest an effective chemical potential near 100 MeV.

Of course other factors affect spectra at low p_t, most noticeably a different collective velocity profile or a different temperature profile. However, proton spectra should be more sensitive to such changes, and it is difficult to imagine how to adjust the profiles to change low-p_t pions while not affecting the nucleons. More sophisticated simulations, where initial conditions are consistent with the geometrical overlap of the incoming nuclei, are necessary to resolve the issue of pion chemical equilibrium. One must also consider that the NA44 experiment has an unusual acceptance where the p_t coverage and the rapidity coverage are correlated leading to a systematic uncertainty not shown in Fig. 5. Although experimental π^+ spectra were used to make the comparison, the π^- spectra were almost identical [14], although a separate NA44 publication [18] reports a significant difference in the low p_t behavior of positive and negative pions.

VII. EVAPORATION AND THE ASSUMPTION OF SIMULTANEOUS BREAKUP

As shown in the literature and in the previous sections of this paper, thermal models are useful in explaining gross features of data and in inferring quantities like the final explosive energy. However, these inferences are based on the assumption of simultaneous breakup. In this section we investigate the validity of this assumption in the context of a thermal model with evaporation and in the context of the cascade.

Our first goal is to understand to what degree evaporation plays a role in the emission of particles from the surface of an expanding fireball. Thermal model fits lead to source sizes which are much larger than the initial projectile and target nuclei. During the time a system expands, some fraction of the system's energy should be radiated from the surface. Estimating evaporation is problematic for three reasons.

1. The system's temperature should be falling during the expansion.
2. The temperature of the surface might be lower than the surface of the interior.
3. The emissivity of the evaporation could easily be less than unity, especially at late stages of the expansion, when time-reversal arguments used to derive evaporative expressions are questionable.

Despite these and other questions, we can still make confident qualitative conclusions. In Fig. 6 pion spectra are shown for a thermal model where evaporation from the surface has been included. The breakup temperature was chosen to be 120 MeV and the final size was determined to fit the dE_t/dy result from CERN as mentioned in section II. Approximately 25% of the pions produced in the collisions are the result of evaporation. Since evaporated particles, by definition, move faster than the surface; they raise the apparent temperature of the overall spectra. This significantly affects the conclusions regarding the collective explosive flow as discussed in sectionV.

Although the qualitative features of Fig. 6 are robust, the strength of the evaporative component might be rather different. If a higher temperature were used, or if the expansion were given time to accelerate, the evaporative component would be larger. Incorporating the correct emissivity might significantly lower the contribution. Microscopic simulations provide the only avenue for a more confident analysis.

Since pions are the lightest hadron, one expects them to comprise the bulk of evaporated particles. Even for pions, it does appear that the majority of emissions occur rather suddenly at the end of the collision. For more massive particles, this would be more true. Thus the idea of a sudden breakup is approximately correct, but the emission of 25% of the pions at earlier times does have a significant effect on the spectra.

We now focus on the the same issue using the vocabulary of cascades. In a cascade description of an exploding system, it is impossible to precisely separate the evaporative component of the emission. One can however get a feel for the simultaneity of the breakup by viewing the distribution of last interactions for various species binned by time.

The upper panel of Fig. 7 shows the distribution of final Bjorken times, $\tau_z = (t^2 - z^2)$ for last interactions of emitted nucleons and pions within a half unit of rapidity from mid-rapidity. The cascade was fed by a thermal model with a 160 MeV temperature input. The feeding was completed by $\tau_z \approx 7$ fm/c. It is clear that nucleons are emitted at later times than pions. This is due to the facts that nucleons have larger cross sections and that nucleons are slower, hence they remain in the dense region for a longer period of time [19]. This latter effect is related to the fact that pions are more likely to evaporate than are nucleons.

To understand the time at which spectra are frozen out, we run the cascade under the same conditions as mentioned above, with the extra condition that no collisions are allowed after a Bjorken time τ_{max}. The average transverse energy of mid-rapidity pions and nucleons are shown as a function of τ_{max} in the lower panel of Fig. 7. The nucleons continue to gain energy after the bulk of particles have been emitted.

Thus it appears that if one wishes to understand the spectral behavior to better than the 20 MeV level, one must abandon simple thermal models based on sudden breakup.

Given the inherent difficulty in evaporative phenomena discussed above, one must resort to simulations in order to investigate the breakup stage.

VIII. SENSITIVITY TO CROSS-SECTIONS

Much of the colliding in the cascade description occurs when hadronic densities are greater than one tenth per cubic Fermi. At these densities in-medium effects can change both single particle properties such as masses and two-particle properties such as the cross section. It is the purpose of this section to investigate the sensitivity of observables to the cross section, by performing an identical analysis for the BNC (thermal+cascade) model with elastic cross sections doubled. Inelastic cross sections were not modified since the principle of detailed balance would be compromised. With unmodified cross sections, half of all collisions are of the elastic nature as opposed to proceeding through resonance formation and decay.

Fig. 8 displays proton spectra from the thermal+cascade calculation using 160 MeV as the initial temperature with both the usual cross section (8, 12 and 16 mb for hadron-hadron, hadron-baryon and baryon-baryon) and doubled cross sections. Since parameters were chosen (see Table III) to fit pion spectra, producing identical pion spectra are not surprising. However, it is noteworthy that the proton spectra in Fig. 8 appear indistinguishable. This demonstrates the relative insensitivity of single-particle spectra to the cross section.

Gaussian source sizes extracted from fitting correlation functions are displayed in Fig. 9. They are compared to the same calculations without double cross sections. These calculations demonstrate that correlation functions are also rather insensitive to the inelastic cross section.

IX. LOCAL KINETIC EQUILIBRIUM

The issue of local thermal equilibration can be divided into two categories of questions. One involves questions of chemical equilibration, which refers to the population of various species. Due to the slow rate of number changing processes compared to the expansion time, chemical equilibrium is expected to quickly disappear during the expansion stage of a collision. However, local kinetic equilibrium can be maintained by any collision, and it is expected that kinetic equilibrium is maintained until shortly before breakup.

It should be emphasized that isotropically expanding collisionless gases maintain local kinetic equilibrium to a high degree. If the velocity gradient is expressed as a time τ, as in Eqs. (4), the momentum of particle with momentum $\mathbf{p}$ as measured in the local frame of the expanding system will cool proportional to $1/\tau$. The apparent temperature will thus fall proportional to $1/\tau$ for an ultrarelativistic gas where $T \propto < |\mathbf{p}| >$ and will proportional to $1/\tau^2$ for a non-relativistic gas where $T \propto < |\mathbf{p}^2|$. Thus the role of collisions is not so much to keep the local velocity distribution of a single species in a thermal form, but to maintain the same local temperature for species with different masses. We therefore will compare local apparent temperatures and expansion velocities of pions and protons.

To determine the local temperature and sidewards velocities of matter at a given position and time, we first consider particles with a specific transverse radius $r_\perp$ at a given Bjorken proper time τ_z. Only particles within a distance of $\tau_z/2$ of the $z = 0$ plane are considered in order to focus on mid-rapidity. For particles in that spatial region, the average outwards momentum $< p_{out} >$ and the root-mean-square sidewards momentum $< p_{side}^2 >^{1/2}$ are calculated. The outwards momentum is the component of the momentum parallel to $\mathbf{r}_\perp$ and the sidewards component is component perpendicular to both the beam axis and to $\mathbf{r}_\perp$. These two quantities are used to determine the average outwards velocity $v_\perp$ and the local temperature T. The extraction is performed by finding $v_\perp$ and T such that:

$$< p_{out} > \; = \frac{1}{I_0} \int p^2 dp d\Omega \exp\left\{ -\frac{\gamma(E(p) - v_\perp p\cos\theta)}{T} \right\} p\cos\theta \qquad (16)$$

$$
\begin{aligned}
< p_{side}^2 > &= \frac{1}{I_0}\int p^2 dp d\Omega \exp\left\{-\frac{\gamma(E(p)-v_\perp p\cos\theta)}{T}\right\}\frac{1}{2}p^2\sin^2\theta \\
I_0 &= \int p^2 dp d\Omega \exp\left\{-\frac{\gamma(E(p)-v_\perp p\cos\theta)}{T}\right\}
\end{aligned}
$$

Local temperatures and velocities are displayed in Fig. 10 as a function of the transverse radius for two times, $\tau = 10$ fm/c and $\tau = 14$ fm/c. At 10 fm/c, collisions are still quite numerous and local temperatures have fallen to around 130 MeV. Both the local temperature and the local collective velocities of pions and protons shown in Fig. 10 are remarkably similar, and the extracted temperatures show very little $r_\perp$ dependence. The small difference in the proton's collective velocities as compared to the pions owes itself to the difficulty in accelerating the more massive protons [19].

At a time, $\tau = 14$ fm/c, the proton's temperature has fallen below that of the pion which is near 100 MeV. This difference is qualitatively what one expects for free streaming particles given that the the proton is non-relativistic while the pions are relativistic. At this time roughly half of all particles have ceased interacting.

By combining the information in Figures 7 and 10, one can reach the conclusion that kinetic equilibrium is maintained until temperatures are near 125 MeV, but that colliding is not really over until temperatures have fallen to near 100 MeV. This suggests that thermal models are rather valid when applied to stages of the collision where temperatures are greater than 130 MeV. However, it is important that one remember that at this stage chemical equilibrium is extremely unlikely, and that subsequent scattering is non-negligible.

X. NUCLEONIC SOURCE SIZES

Aside from the measurements considered thus far, there are a variety of other observables to consider, such as the ratios of chemical species (e.g. K/π), and correlations of particles other than pions. In this section we present predictions for kinematically cut nucleonic source sizes based on coalescence arguments. These quantities are pertinent to the issues of kinetic equilibrium and freeze out. We postpone the investigation of other chemical ratios to a later study.

For nucleon sizes, we again consider the case where thermal particles are created at a temperature of 160 MeV and then propagated with a cascade description. In this case we consider a source size generated via a coalescence prescription [20].

$$R^3(\mathbf{p}) = \frac{3}{4}\pi^{3/2}\frac{\frac{dN_{prot}}{d^3\tilde{p}_\pi}\frac{dN_{neut}}{d^3\tilde{p}_\pi}}{\frac{dN_{deut}}{d^3\tilde{p}_d}} \tag{17}$$
$$d^3\tilde{p} \equiv 2\pi m p_t dp_t dy$$

The momentum of the deuteron p_d should be chosen as twice the momentum of the nucleons such that the nucleons and deuteron move at the same velocity. Deuteron spectra were generated via a coalescence prescription [20,21]. If a cascade generates protons and neutrons at space-time coordinates x_a and x_b with momenta $\mathbf{p}_a$ and $\mathbf{p}_b$, deuterons can be generated via the prescription,

$$\Delta N_{deut} = \frac{3}{4(\sigma\mu)^3}\Sigma_{ab}\exp\left\{-\frac{q^2}{2\sigma^2} - \frac{r^2}{2\mu^2}\right\} \tag{18}$$
$$q^2 \equiv \frac{1}{4}\left\{-(p_b - p_a)^2 + \frac{\left[(p_b - p_a)\cdot(p_a + p_b)\right]^2}{(p_a + p_b)^2}\right\}$$
$$r^2 \equiv -(x_b - x_a)^2 + \frac{\left[(x_b - x_a)\cdot(p_a + p_b)\right]^2}{(p_a + p_b)^2}$$

Here r and q are the relative position and relative momentum of the two nucleons measured in the frame of the nucleons. The results will be independent of σ and μ as long as the they are much smaller than characteristic scales of the spatial and momentum distributions respectively. We chose values of 50 MeV/c for μ and 1.0 fm for σ. Neutron spectra are usually not available experimentally, though they can be estimated by multiplying the nucleon spectra by a constant to account for the neutron excess in the lead target and lead projectile. Since isospin asymmetries are not incorporated in the calculations presented here, the same source sizes are generated for both neutrons and protons.

Nucleonic source sizes are shown in Fig. 11 as a function of the transverse momentum of a nucleon. They are compared to the corresponding radius for pions, which is defined by:

$$R_\pi^- 3(\mathbf{p}_t) = \frac{1}{\pi^{3/2}}\int d^3q_{inv}\left(C(\mathbf{p}_t, q_{inv}) - 1\right), \tag{19}$$

where C is the two-pion correlation function. If m_t scaling were valid, the nucleonic source sizes along the beam axis would be smaller than those for the pions by a factor of the ratio of the pion mass to the proton mass. Since R_{inv} is the geometric mean of the three radii, one would expect that R_{inv} for protons to be smaller by a factor of the cubic root of the ratio of the masses than R_{inv} for pions. This is approximately true.

The flatness of R_{inv} as a function of p_t for protons is also notable. It signifies that the finite lifetime effect that would lead to R_{inv} rising as a function of p_t is balanced by the effects of expansion and cooling which would push R_{inv} to fall as a function of p_t.

XI. CONCLUSIONS

Two categories of conclusions have been reached through this study. The first category can be regarded as lessons for understanding the impact of model parameters and the justification of assumptions used in modeling. The second group of conclusions are those that represent interpretations of experimental results. The first set of conclusions are:

1. Evaporation from an expanding surface noticeably affects pion spectra even though evaporated particles represent a minority of emitted particles.

2. Baryons remain in the collision region a significantly longer time than do pions.

3. Both single-particle spectra and correlation functions are rather insensitive to the size of elastic cross sections used in a cascade description.

4. An initially equilibrated expanding and cooling hadronic gas will lead to a final state with the overall phase space filling approximately 20% over populated.

5. Sidewards collective velocities continue to increase from approximately $0.3c$ to $0.6c$ during the late stage of the collision.

The following conclusions can be made regarding conditions in true collisions.

1. There exists evidence in both the correlation functions and in the shape of the pion spectra at low p_t that the final phase space density for pions is over populated by approximately $80 \pm 20\%$. Experimental correlation functions suggest sizes, that when combined with the measurement of transverse energy and single particle spectra, yield phase space filling factors which are near 0.5.

2. Most matter dissolves in bulk. In the simulations, approximately 25% of the particles can be characterized as being emitted from the surface, while experimental results suggests an even smaller percentage since measurements of R_{out} are closer to R_{side} than are the predictions presented here.

3. A small fraction of the total energy can be considered as sidewards collective energy since sidewards collective velocities are relatively small compared to the typical thermal velocities for pions.

Unfortunately, more firm quantitative conclusions should not be made at this stage of the study. In order to make stronger conclusions, one must improve the model by increasing the list of included processes, understanding the sensitivity to more realistic density and collective velocity profiles, and considering more measurements such as those involving kaons and hyperons. Even should the model be improved and better studied, one important lesson gained from this analysis is that chemical equilibrium for pions is probably lost when the temperatures are at or above 160 MeV and hadronic densities are near 0.5 per cubic fm. At these densities, the properties of hadrons are certainly quite different than vacuum properties, and the interpretation of the earlier stages based on modeling hadronic evolution is questionable.

On the positive side, it should be emphasized that even though chemical equilibrium appears lost at an early stage of the collision, kinetic equilibrium appears to be a good approximation for temperatures above 130 MeV. This suggests that it is an attainable goal to describe the system in terms of a temperature, chemical potentials and fugacities when the system has a temperature near 140 MeV since few particles have escaped before that time. Firmly understanding the state of the system at one time, when microscopic quantities like temperature and chemical potentials are still meaningful, would represent a significant success for the phenomenology of relativistic heavy ion collisions. Such knowledge would provide an invaluable boundary condition for the modeling of earlier stages of the collision.

ACKNOWLEDGMENTS

This work was supported by the National Science Foundation under grants PHY-9513900, PHY-9403666 and PHY-9605207.

REFERENCES

[1] T. Peitzmann, et al., Nucl. Phys. **A610**, 200c (1996).

[2] S. Margetis, et al., Nucl. Phys. **A590**, 355c (1995).

[3] P.G. Jones, et al., Nucl. Phys. **A610**, 188c (1996).

[4] G.Q. Li, C.M. Ko, and G.E. Brown, Phys. Rev. Lett. **75**, 4007 (1995); G.Q. Li, C.M. Ko, and G.E. Brown, Nucl. Phys. **A606**, 503 (1996).

[5] U. Mayer and U. Heinz, Phys. Rev. C**56**, 439 (1997).

[6] P. Braun-Munzinger, J. Stachel, J.P. Wessels and N. Xu, Phys. Lett. **B365**, 1 (1996).

[7] J. Rafelski, Acta Phys. Polonica **27**, 1037 (1996).

[8] U. Heinz, Nucl. Phys. **A566**, 205c (1994); E. Schnederman and U. Heinz, Phys. Rev. C**50**, 1675 (1994); E. Schnederman and U. Heinz, Phys. Rev. C**47**, 1738 (1993); E. Schnederman and U. Heinz, Phys. Rev. Lett. **69**, 2908 (1992);

[9] B. Tomášik and U. Heinz, LANL report nucl-th/9707001 (1997).

[10] H. Sorge, H. Stöcker and W. Greiner, Ann. Phys. **192**, 266 (1989).

[11] K. Werner, Phys. Rep. **232**, 87 (1993).

[12] L.V. Bravina, I.N. Mishustin and J.P. Bondorf, Phys. Lett. **B354**, 196 (1995).

[13] P. Danielewicz and S. Pratt, Phys. Rev. **C53**, 249 (1996).

[14] I.G. Bearden eta al., "Collective expansion in high Energy Heavy Ion collisions", Phys. Rev. Lett., in press.

[15] S. Gavin and V. Ruuskanen, Phys. Lett. **B262**, 326 (1991); S. Gavin, Nucl. Phys. **B351**, 561 (1991).

[16] C. Greiner, C. Gong and B. Müller, Phys. Lett. **B316**, 226 (1993).

[17] G.F. Bertsch, Phys. Rev. Lett. **72**, 2349 (1979).

[18] H. Bøggild, et al., Phys. Lett. B372, 339 (1996).

[19] H. Sorge, Phys. Lett. **B373**, 16 (1993).

[20] W.J. Llope, et al., Phys. Rev. C**52**, 2004 (1995).

[21] R. Mattiello, H. Sorge, H. Stöcker and W. Greiner, Phys. Rev. C**55**, 1443 (1997).

TABLES

π^+	π^-	π^0	η	η'	K^+	K^-	K^0	$\overline{K}^0$	ρ^+	ρ^-	ρ^0	ω	K^{+*}	K^{-*}	K^{0*}	$\overline{K}^{0*}$	ϕ
139	139	135	549	958	494	494	497	497	770	770	770	782	892	892	896	896	1019

TABLE I. Meson list

Λ	n	p	Σ^+	Σ^0	Σ^-	Ξ^0	Ξ^-	Δ^{++}	Δ^+	Δ^0	Δ^-	Σ^{+*}	Σ^{0*}	Σ^{-*}	Ξ^{0*}	Ξ^{-*}	Ω^-
1116	940	938	1189	1193	1197	1315	1321	1232	1232	1232	1232	1383	1384	1387	1530	1530	1673

TABLE II. Baryon list

model, temperature (MeV)	$v_{\perp,\max}$	μ_b (MeV)	τ_b (fm/c)	$v_{z,\max}$
thermal, T=100	0.75	335	13.55	0.980
thermal, T=120	0.646	275	10.7	0.976
thermal, T=140	0.550	225	8.15	0.972
+evaporation, T=100	0.606	335	16.45	0.955
+evaporation, T=120	0.480	272	13.12	0.946
+evaporation, T=140	0.371	225	9.92	0.935
+cascade, T=120	0.480	275	13.16	0.945
+cascade, T=140	0.362	225	10.1	0.933
+cascade, T=160	0.300	190	7.00	0.929
double σ, T=160	0.305	190	6.91	0.925

TABLE III. Input parameters for the 10 cases used in this study.

FIGURES

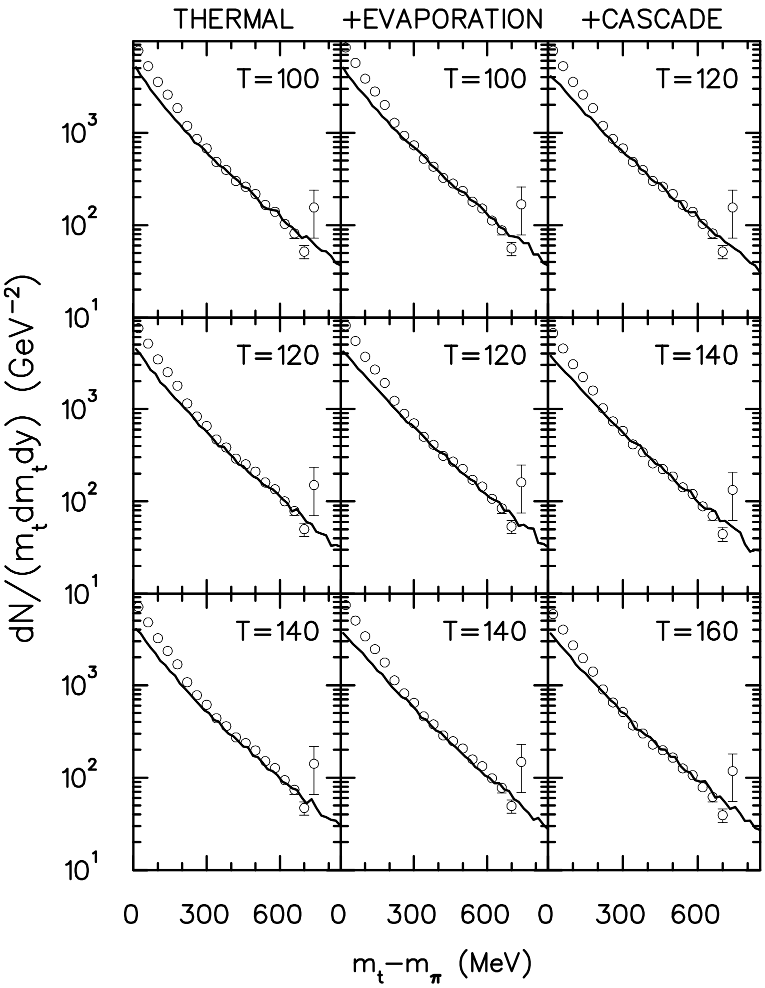

FIG. 1. Pion spectra derived from each of the three cases are shown for several breakup temperatures, and compared to experimental results of the NA44 collaboration(circles). The left-most panels show results of a simple thermal model where evaporation is neglected. The center panels present spectra for a thermal model where evaporation is included and the calculations shown in the right-most panels included the cascade (BNC model).

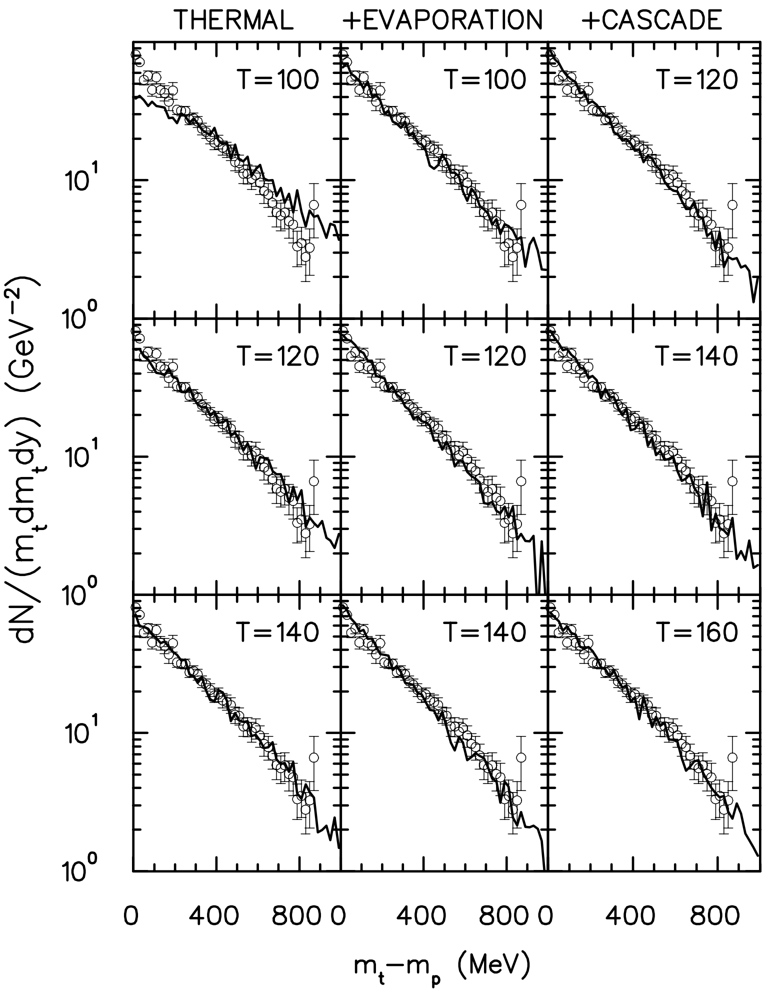

FIG. 2. Proton spectra derived from each of the three cases are shown for several breakup temperatures, and compared to experimental results of the NA44 collaboration(circles). The left-most panel shows results of a simple thermal model where evaporation is neglected. The center panel presents spectra for a thermal model where evaporation is included and the calculations shown in the right-most panel included a cascade treatment of particles after their creation.

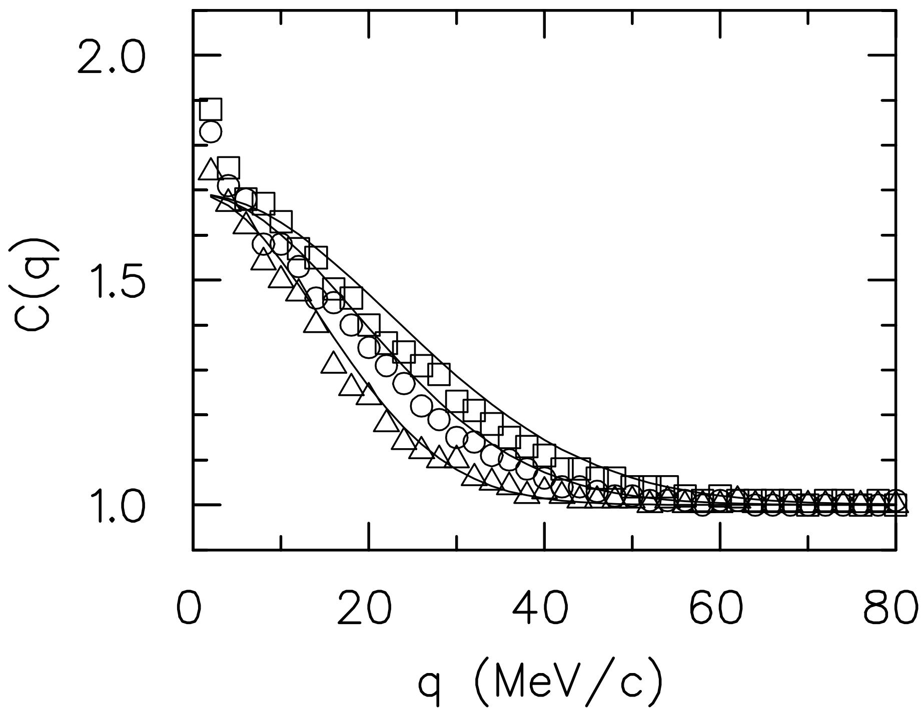

FIG. 3. Pion correlation functions are shown for mid-rapidity pion pairs with average $\bar{p}_t$ of 150 MeV/c. Sidewards (squares), outwards (circles) and beam (triangles) directional cuts were made and compared to the Gaussian parameterization (lines).

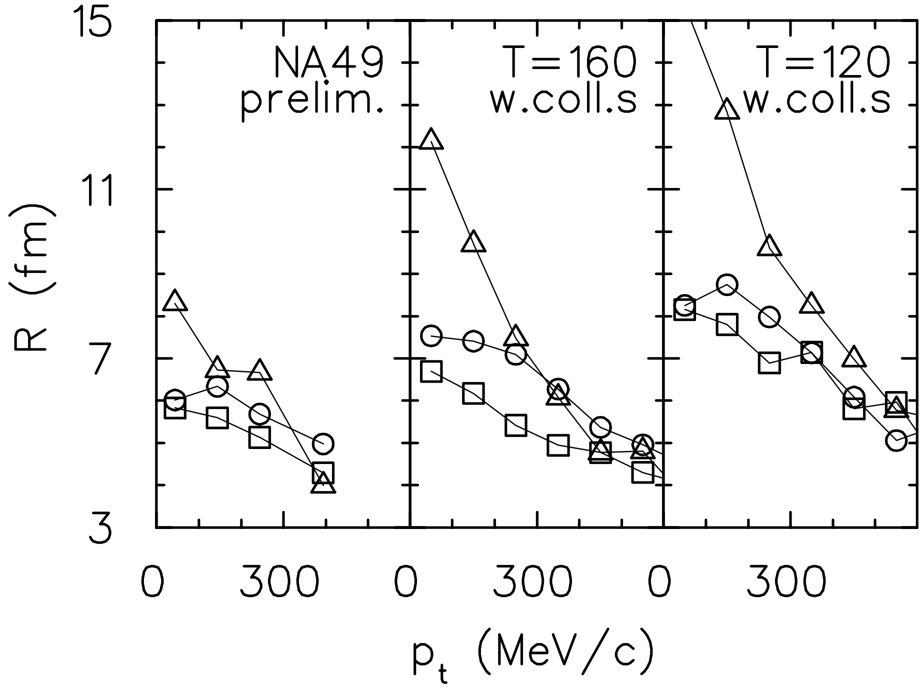

FIG. 4. Gaussian source radii are shown as a function of $\bar{p}_t$, the average momentum of the pion pair, for mid-rapidity pions. Sidewards (squares), outwards (circles) and beam (triangle) dimensions are displayed for calculations of thermal model where subsequent interactions were handled by a cascade. The thermal+cascade model with T=160 MeV (center panel) leads to smaller source sizes than the same model with T=120 MeV.

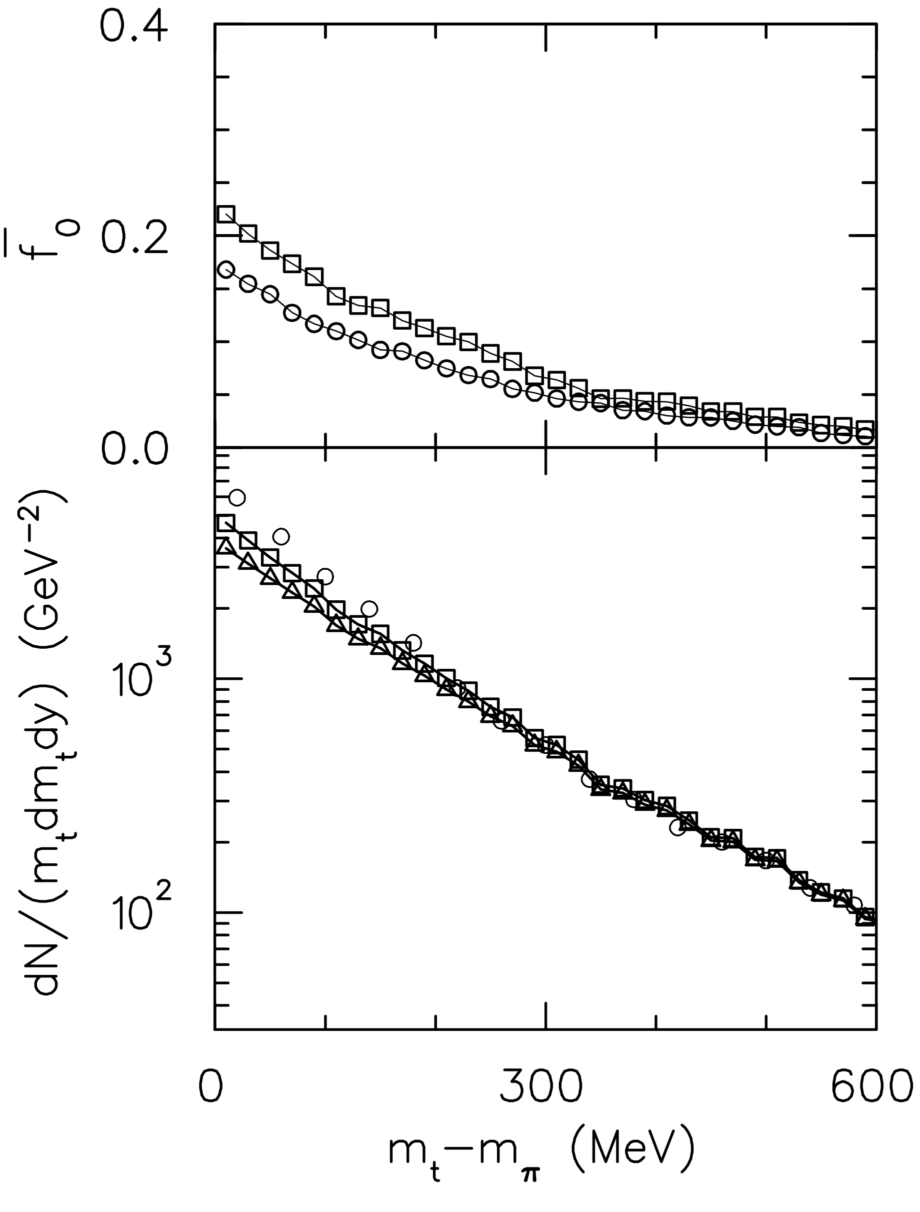

FIG. 5. Effective phase space filling factors for pions are shown as a function of the transverse mass in the upper panel for the BNC model (thermal+cascade) with a temperature $T = 160$ MeV (squares) and $T = 120$ MeV (circles). Bose corrections to the spectra are illustrated in the lower panel, by displaying both uncorrected (triangles) and Bose-corrected (squares) results for the T=160 MeV case. They are compared to NA44 π^+ spectra (circles).

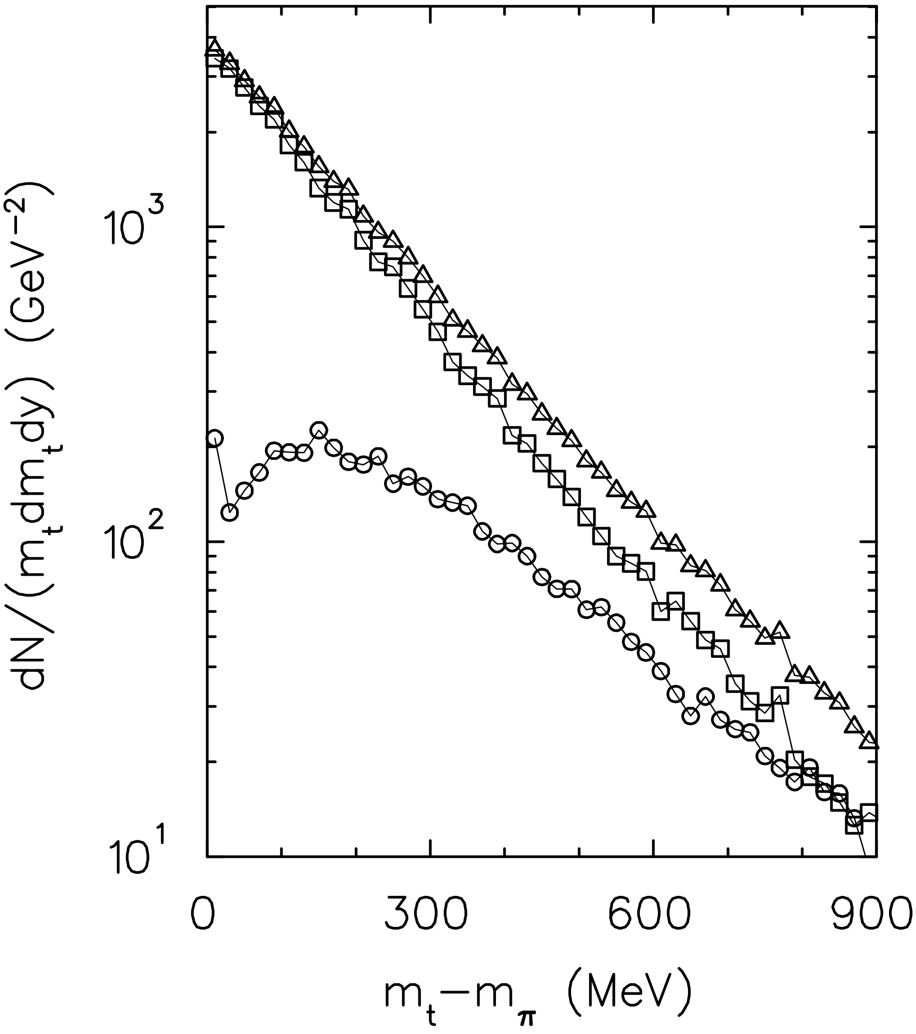

FIG. 6. For the thermal+evaporation model with a breakup temperature of 120 MeV, pion spectra are divided into their evaporative component (circles), the component due to final breakup (squares) and the sum (triangles). Although the majority of pions are emitted suddenly at the end of the collision, the evaporative component significantly affects the shape of the spectra.

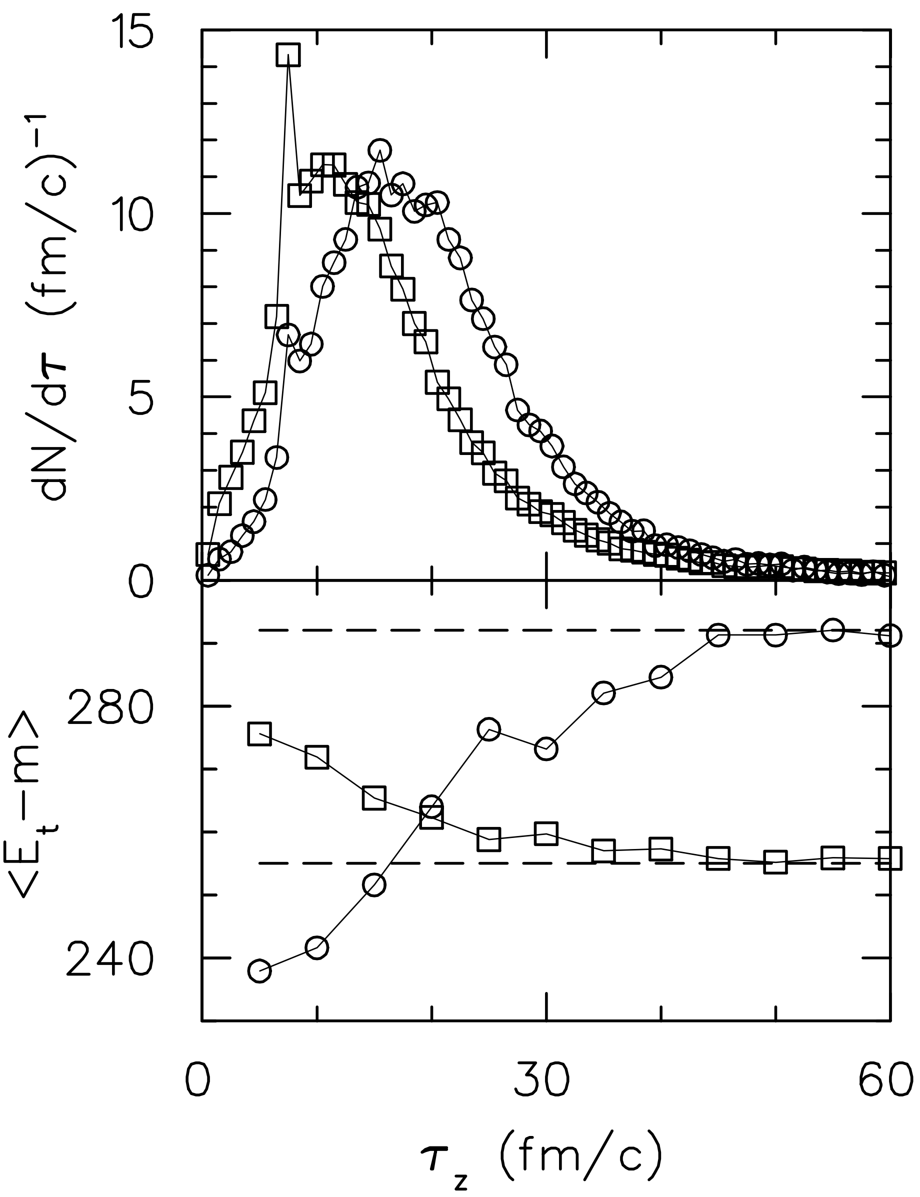

FIG. 7. Distributions for final proper times, τ_z, for final collisions of emitted pions (squares) and emitted nucleons (circles) are shown in the upper panel. Calculations used the BNC (thermal+cascade) model with a creation temperature of 160 MeV. The lower panel displays the mean transverse energy of emitted pions (squares) and nucleons (circles) as a function of turning of all collisions after a proper time τ_z. Asymptotic values are shown with dashed lines. These plots indicate that nucleons are emitted later than pions and that nucleons continue to accelerate and gain transverse energy at the expense of the pions. Pions have been scaled down by a factor of seven.

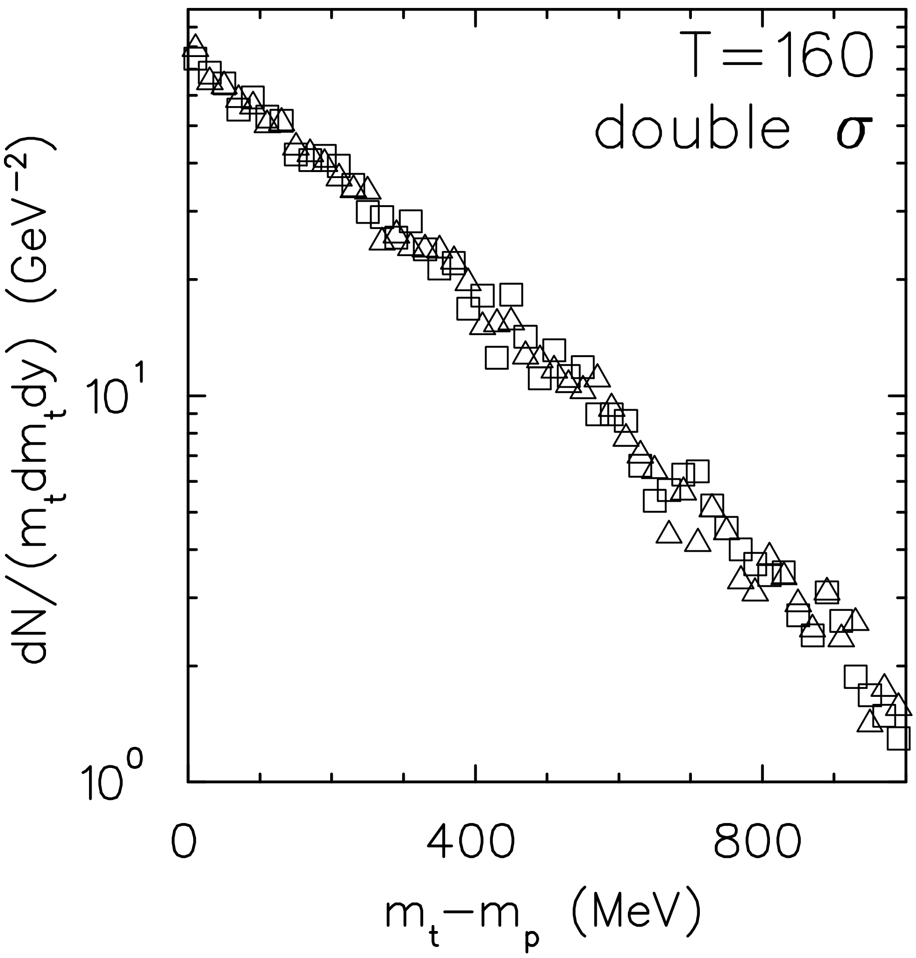

FIG. 8. Proton spectra for the thermal+cascade model with the input thermal spectra generated with a 160 MeV temperature. Calculations performed with elastic cross-sections of 8, 12 and 16 mb (squares) with doubled cross sections (triangles). Since parameters were adjusted to fit the pion spectra, this demonstrates the insensitivity of single-particle spectra to cross-sections.

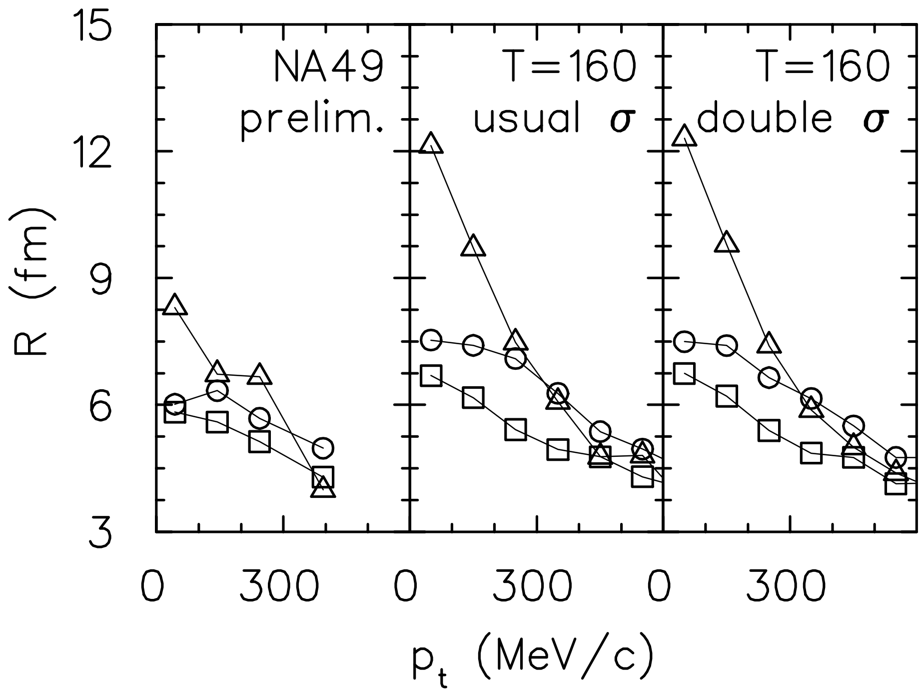

FIG. 9. Gaussian source sizes extracted by fitting correlation functions for mid-rapidity pions are displayed as a function of transverse mass. Thermal+cascade model results are displayed in the center based on a temperature of 160 MeV. The right-side panel shows results for the same model, but with doubled elastic cross sections. This shows the sensitivity of the correlation results to the cross sections. Preliminary NA49 results are displayed in the left-side panel. Gaussian sizes are displayed for three directions, outwards (circles), sidewards (squares) and beam (triangles).

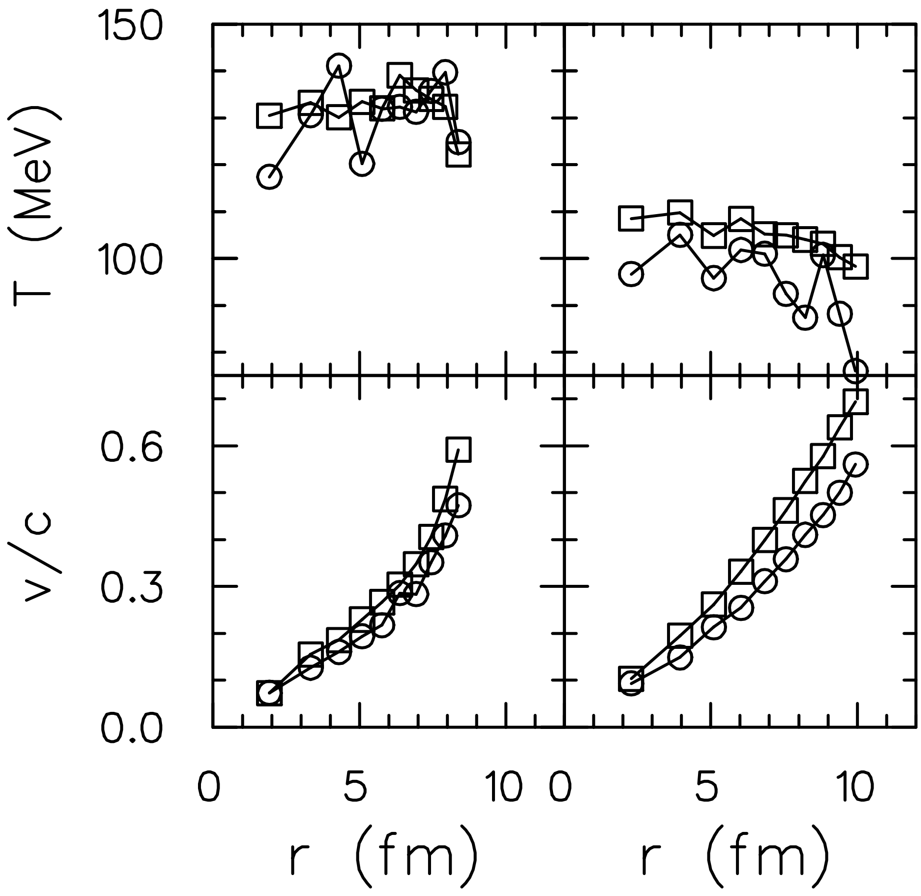

FIG. 10. The upper panels display local temperatures as a function of the radius of the expanding matter for proper times $\tau = 10$ fm/c (left) and $\tau = 14$ fm/c (right) for pions (squares) and protons (circles). The lower panels display collective velocities at the same times. This demonstrates that kinetic equilibrium is maintained between pions and protons until the temperature falls below 130 MeV.

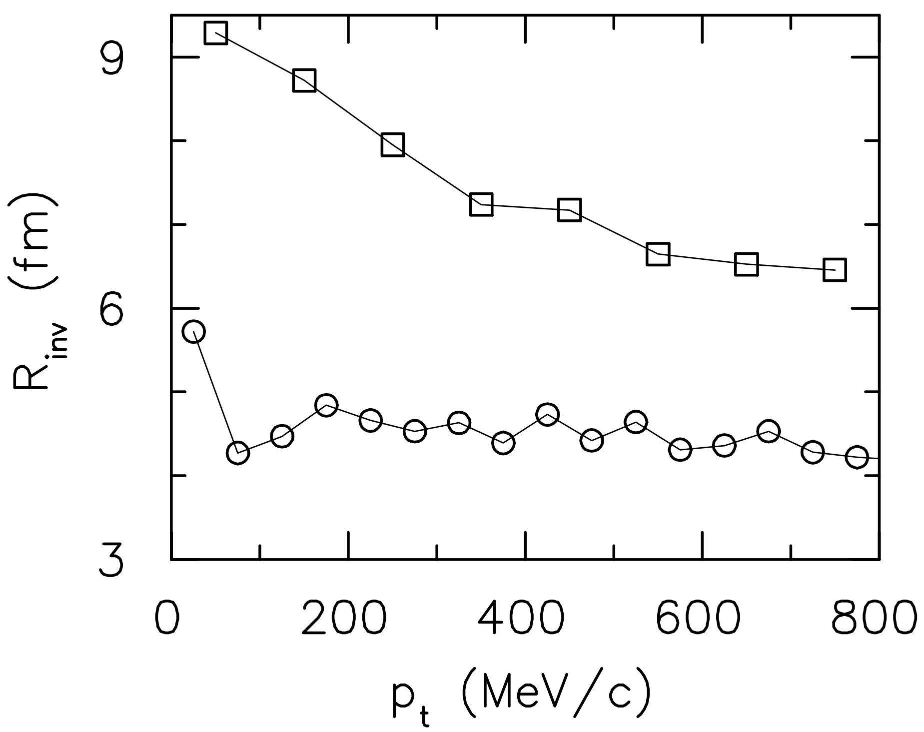

FIG. 11. The effective Gaussian size, R_{inv}, is shown as a function of p_t for both pions and nucleons for the BNC (thermal+cascade) model using a temperature of 160 MeV. These results are consistent with arguments based on sudden breakup of Bjorken geometries (M_t scaling) would suggest that at zero p_t, the pion and nucleon sizes would be related by the cube root of their masses.